Chaotic Polarization-Assisted *L*DPSK-MPPM Modulation for Free-Space Optical Communications

Abdulaziz E. Elfiqi, *Member, IEEE*, Haitham S. Khallaf, Salem F. Hegazy, Amr Elsonbaty, Hossam M. H. Shalaby, *Senior Member, IEEE*, and Salah S. A. Obayya, *Senior Member, IEEE*

***Abstract*— In this paper, we present a polarization-assisted *L*-ary differential phase-shift keying multipulse pulse-position modulation (PA.*L*DPSK-MPPM) technique that is secured in the physical layer by a discrete-chaos system. The all-optical PA.*L*DPSK-MPPM scheme benefits from the polarization as an additional degree of freedom which greatly reduces the system complexity relative to prior implementations. The discrete-chaos scrambling is based on a message-seeded two-dimensional chaotic map tailored for independent perturbation of the occupied time-slot positions (MPPM information) and their relative phase shift (*L*DPSK information). Synchronized and non-synchronized implementations of the chaotic PA.*L*DPSK-MPPM technique are proposed with expressions for the corresponding spectral efficiencies being determined and compared with prior *L*DPSK-MPPM setups. The performance of PA.*L*DPSK-MPPM under gamma-gamma (GG) free-space optical (FSO) fading channels is analytically verified to outperform the prior designs for different FSO channel states which is supplemented by Monte Carlo (MC) simulations. The system security is numerically examined against various types of attacks, including brute-force, differential, and statistical attacks.**

Manuscript received April 25, 2018; revised September 29, 2018 and March 3, 2019; accepted May 25, 2019. Date of publication June 12, 2019; date of current version September 10, 2019. This work was supported in part by the National Telecommunication Regulatory Authority (NTRA), Ministry of Communication and Information Technology, Egypt. The associate editor coordinating the review of this paper and approving it for publication was M. S. Alouini. *(Corresponding author: Salah S. A. Obayya.)*

A. E. Elfiqi is with the Electronics and Electrical Communications Engineering Department, Faculty of Electronic Engineering (FEE), Menoufia University, Menouf 32952, Egypt (e-mail: abdulaziz.elfiqi@ieee.org; abdulaziz.elfiqi@el-eng.menofia.edu.eg).

H. S. Khallaf is with the Department of Electrical and Electronics Engineering, Ozyegin University, 34794 Istanbul, Turkey, on leave from the Nuclear Research Center, Egyptian Atomic Energy Authority (EAEA), Inshas 13759, Egypt (e-mail: haitham.khallaf@ozyegin.edu.tr).

S. F. Hegazy is with the National Institute of Laser Enhanced Sciences, Cairo University, Giza 12613, Egypt, and also with the Center for Photonics and Smart Materials, Zewail City of Science and Technology, Giza 12578, Egypt (e-mail: shegazy@zewailcity.edu.eg).

A. Elsonbaty is with the Mathematics Department, College of Science and Humanities Studies, Prince Sattam Bin Abdulaziz University, Al-Kharj 11942, Saudi Arabia, also with the Department of Mathematics and Engineering Physics, Faculty of Engineering, Mansoura University, Mansoura 35516, Egypt, and also with the Center for Photonics and Smart Materials, Zewail City of Science and Technology, Giza 12578, Egypt (e-mail: aturkey@zewailcity.edu.eg).

H. M. H. Shalaby is with the Electrical Engineering Department, Alexandria University, Alexandria 21544, Egypt, and also with the Department of Electronics and Communications Engineering, Egypt-Japan University of Science and Technology (E-JUST), Alexandria 21934, Egypt (e-mail: shalaby@ieee.org).

S. S. A. Obayya is with the Center for Photonics and Smart Materials, Zewail City of Science and Technology, Giza 12578, Egypt (e-mail: sobayya@zewailcity.edu.eg).

Color versions of one or more of the figures in this paper are available online at http://ieeexplore.ieee.org.

Digital Object Identifier 10.1109/TWC.2019.2920970

***Index Terms*— Chaos-based communications, differential phase-shift keying (DPSK), discrete chaos, free-space optics (FSO), multipulse pulse-position modulation (MPPM), physical encryption.**

I. Introduction

In the past decades, free-space optical (FSO) communication has attracted growing interest driven by its unique features like huge transmission capacity, low required power, free-licensing, and cost effectiveness [1], [2]. Hybrid modulation techniques have been widely used to improve the poor power efficiency of high-order spectrally-efficient modulation techniques and to maximize the benefits of FSO transmission [3]–[15].

Quite recently, a proposal of all-optical direct-detection-based hybrid modulation combining differential phase-shift keying with multipulse pulse-position modulation (DPSK-MPPM) has been proposed [9], accompanied with a thorough analysis for its amplifier-limited performance. In addition, the performance of the hybrid DPSK-MPPM technique has been evaluated over a long-haul, nonlinear, and dispersive fiber-optic channel [10]. However, in these works, the DPSK-MPPM modulation technique requires equipping the transmitter and receiver with two multi-stage optical-delay lines to add and restore the delay without perturbing the phase information. The necessary condition of no-phase-perturbation has been satisfied in [9] at the cost of increasing system complexity through constraining perfect matching between multi-stage delay lines at transmitter and receiver. In [10], a reconciliation routine has been considered in order to insure no-phase-perturbation, but this routine needs to be done periodically to compensate for random phase fluctuations.

On the other hand, the protection of critical information in modern wireless communication against snooping has recently received great interest [16]. The security of computationally-hard public-key cryptosystems, such as RSA algorithm [17], becomes *day-after-day* less effective due to the growing computational power, as well as the accelerating advances in quantum computation technology [18], [19]. The proposed DPSK-MPPM systems so far assume unsecured communication channel, however, securing the hybrid-modulation channel on the physical level can be done for additional system complexity. New strategies have been proposed for the sake of improving security strength and confidentiality of transmitted information [20], where substantial security level can be achieved when the encoding process is fulfilled in

the physical layer of the communication network protocol. In particular, in chaos-based cryptography, the chaotic signal is generated and utilized in the physical layer instead of manipulating the digital data algorithmically [21]. Moreover, discrete-time chaotic systems have the unique feature of being easily implementable on available digital platforms like digital signal-processing units [20], [22], [23].

In this paper, we propose a chaos-secured polarization-assisted L-ary differential phase shift keying-multipulse pulse-position modulation (PA.LDPSK-MPPM) that benefits from the polarization of the optical signal and the discrete chaos to eliminate such system complexities and to incorporate a high level of information security. The key idea is to encode LDPSK continuously along a frame of N time-slots. The MPPM is encoded by distributing w *active* time-slots of a specific linear polarization, while the rest of $N-w$ time-slots having the orthogonal polarization. The simple idea of polarization orthogonality allows for continuous LDPSK encoding without breaking the frame into occupied and dark time slots for MPPM encoding as done in former works [9], [10]. In this sense, the suggested system does not only boost the LDPSK information rate but also dispenses with the bulky phase-preserving multi-stage optical-delay lines at the channel terminals that are required in [9], [10]. Besides its obvious simplicity, the PA.LDPSK-MPPM approach is verified to provide a comparable spectral efficiency to that of the prior setups in [9] and [10].

The appealing applications for the proposed chaotic PA.LDPSK-MPPM modulation technique extend from short- to medium-range optical wireless communication (see, e.g., [24]). For instance, it is desired for the optical wireless sensor networks that send critical information in industrial and nuclear plants to use highly secured low-power and low-complexity communication systems [25]. Another attractive application is the inter-vehicle communication systems where a portion of information is delay-sensitive which can be carried over the MPPM frames (e.g., information for collision avoidance). The other information portion that requires higher data rate yet less sensitive to time delay can be sent over LDPSK part [26].

The main contributions in this paper are summarized as follows.

- We propose *simple-structured* setups for chaotic hybrid polarization-assisted L-ary differential phase shift keying-multipulse pulse-position modulation (PA.LDPSK-MPPM) technique based on the manipulation of light polarization as an additional degree of freedom.
- A message-seeded variant of the two-dimensional Zaslavsky map is introduced to ensure the independent security of the discrete-chaos-based PA.LDPSK-MPPM scheme in the w active slot-positions and their differential phase.
- The spectral efficiencies for hybrid LDPSK modulation techniques are determined and compared.
- Closed-form expressions for upper-bound bit-error rate (BER) under gamma-gamma (GG) turbulence FSO channel are derived with the PA.LDPSK-MPPM system performance being compared with the more complicated setups in [9], [10].
- Closed-form BER expression for the chaos effect on the bit error performance is derived and explained.
- As a proof of concept, a secure transmission of an image message is numerically demonstrated. Security analysis is carried out in order to inspect the immunity of the proposed secure data transmission scheme to various types of possible attacks.

The rest of the paper is organized as follows. In Section II, the related works for both hybrid modulation and chaotic modulation encryption are explored. In Section III, different proposed setups for the PA.LDPSK-MPPM scheme are detailed. Furthermore, the chaotic perturbations in position and phase are proposed. In Section IV, the spectral efficiencies of proposed systems are determined. The BER performance under GG turbulence FSO channel are derived and discussed and the chaos effects on the BERs are investigated in Section V. In Section VI, results and discussions are presented. Finally, the conclusion is given in Section VII.

II. Related Works

The idea of integrating two ordinary modulation techniques into a hybrid technique merging their advantages has recently attracted much interest [3]–[14]. A hybrid modulation technique based on combining M-ary pulse-position modulation (M-PPM) or M-ary frequency-shift keying (M-FSK) with additional polarization and/or phase modulation which enables boosting the receiver sensitivity has been introduced by Liu *et al.* [4]. Hybrid modulation based on polarization-switched quadrature phase-shift keying (PS-QPSK) and polarization-division multiplexing quadrature phase-shift keying (PDM-QPSK) superimposed on pulse-position modulation (PPM) has been proposed and investigated in [3], [5], [6]. Another hybrid modulation technique based on combining multiple-pulse pulse-position modulation (MPPM) with binary phase-shift keying (BPSK) or quadrature-phase shift keying (QPSK) has been proposed in [7]. Also, a hybrid modulation technique based on both orthogonal frequency-division multiplexing and pulse-position modulation (OFDM-PPM) has been proposed in [8]. In [14], [27], L-ary quadrature-amplitude modulation with multiple-pulse pulse-position modulation (LQAM-MPPM) has been introduced based on subcarriers intensity modulation, while carrying out LQAM modulation and demodulation processes in the electrical domain. In [9], [10], a hybrid differential phase-shift keying multi-pulse pulse-position modulation (DPSK-MPPM) technique has been proposed and investigated. Although, it is a direct-detection based system, the scheme involves the challenging match of optical paths in two controllable multi-stage optical-delay lines used by the two communicating parties.

The fascinating features of optical chaos, like its random-like behavior and wide-band spectrum, have attracted increasing interest as an efficient and versatile tool for secure data communication [28]–[31], physical-image encryption [32]–[36], physical ultra-fast random number generators [37]–[40], chaotic lidar [41], and optoelectronic logic gates [42]. Several optical realizations for

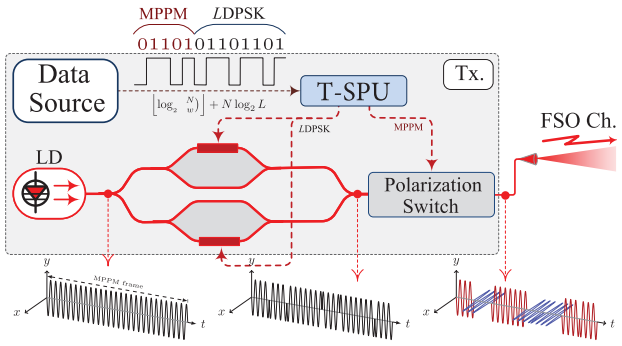

Fig. 1. Schematic showing the PA.*L*DPSK-MPPM transmitter with $N = 8$, $w = 3$, and $L = 2$. LD labels the laser diode, T-SPU denotes the transmitter signal-processing unit, Tx. denotes the transmitter terminal, and FSO Ch. denotes free-space optical channel.

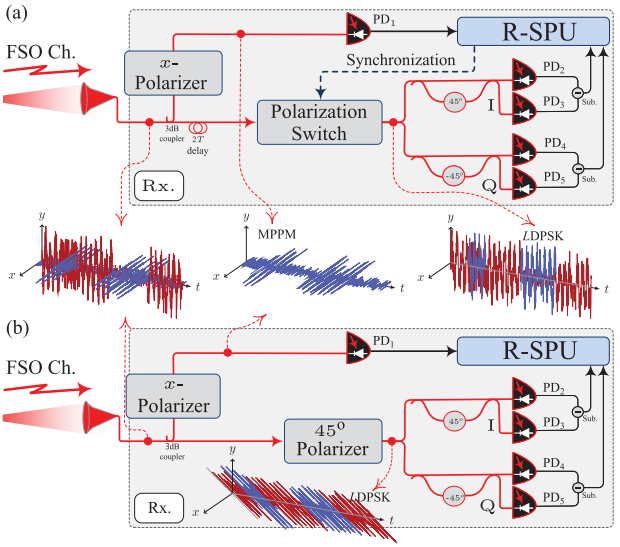

Fig. 2. Schematic setups of the PA.*L*DPSK-MPPM receivers with $N = 8$, $w = 3$, and $L = 2$: (a) Synchronized implementation and (b) non-synchronized implementation. $x-$ and 45° polarizers transmit light polarized at x-axis and diagonal directions, respectively. PD labels the photodetector, R-SPU denotes the receiver signal-processing unit, Rx. denotes the receiver terminal, and FSO Ch. denotes free-space optical channel, I denotes the in-phase, Q denotes the quadrature, T is MPPM frame duration, Sub. denotes the subtractor, and 45° and -45° are phase shifter over I and Q branches, respectively.

continuous-time chaotic systems have been verified to be ultimately secure by simultaneous concealment of the time-delay signature in all observables i.e. in intensity and phase of chaotic output. For example, a new hybrid feedback scheme is proposed to conceal time-delay signature in the chaotic output of a single Vertical Cavity Surface Emitting Laser (VCSEL) diode [43] and metal cladding nanolaser [44]–[46].

The ultimate goal of chaos modulation techniques is to realize low-power and low-complexity communication systems of excellent anti-fading and anti-intercept capabilities. Due to this goal, the chaos has been depicted in different modulation schemes. Examples of these techniques include chaotic on-off-keying (COOK) [47], chaotic pulse-position modulation (CPPM) [22], chaos shift keying (CSK) [48], and quadrature CSK [49]. Furthermore, the non-coherent chaotic schemes such as: differential chaos shift keying (DCSK) in [50], L-ary DCSK [51], improved differential chaos-shift keying (I-DCSK) [52], and short reference DCSK (SR-DCSK) [53]. Recently, an improved energy-efficient non-coherent permutation index differential chaos shift keying (PI-DCSK) modulation scheme is proposed in [54].

III. Proposed PA.*L*DPSK-MPPM Setups

In this section, we present the transmitter model of PA.*L*DPSK-MPPM system along with the synchronized and non-synchronized variants of the receiver model.

A. Transmitter

Consider an LDPSK-MPPM encoding system with L being the cardinality of the constellation of LDPSK, and N and w being the number of available MPPM time slots and occupied signal time slots, respectively. Figure 1 shows the schematic of the chaotic PA.LDPSK-MPPM transmitter. A raw data frame of $\lfloor \log_2 \binom{N}{w} \rfloor$(MPPM bits) $+Nm$ (PA.LDPSK bits) is fed to the transmitter signal-processing unit (T-SPU), where $m = \log_2 L$ and $\lfloor z \rfloor$ is the floor integer of z. For secure transmission, a routine run by the T-SPU executes a message-seeded two-dimensional chaotic map (discussed later in III-D) to scramble the raw data frame. The T-SPU delivers the chaos-perturbed phase and MPPM bits to an LDPSK modulator and polarization switch, respectively. The former modulates the phase of the input continuous wave (CW) laser beam which is linearly-polarized along y-axis. The latter flips the polarization of w time slots out of N time slots, therefore only w time slots is x-polarized, while the polarization of the other time slots remains unchanged. Among the different degrees of freedom of light [55], [56], there are several advantages for using the state of polarization as the ancillary degree of freedom; most importantly, the availability of commercial high-speed polarization switches with rates up to $10\times$ GHz (see for example [57]). Furthermore, the manipulation / measurement of the polarization state is simple and precise using the available wave plates and polarizers. The phase- and polarization-modulated light beam is then directed through FSO channel where it is subjected to channel effects.

B. Synchronized Receiver

A schematic of the synchronized receiver is depicted in Fig. 2(a). The received signal is split into two distinct arms prepared for MPPM and LDPSK demodulation using the 3 dB coupler (upper and lower arms, respectively). In the MPPM arm, a photodetector measures the light intensity over the N time slots after passing through an x-polarizer. A soft decision is then made regarding the positions of the most intense w time slots out of N stored values. The synchronized scheme requires prior knowledge on the positions of w most-occupied slots before decoding the phase information. Therefore, a two frames length delay loop on the LDPSK arm postpones the processing of the phase information until the active w time slots are identified. The receiver signal-processing unit (R-SPU) is then able, using a polarization switch, to counteract the polarization flipping along the optical frame to

be again unified along y-axis. The unification of the polarization enables the decoding of the differential phase information via interference between two subsequent signal slots on τ-unbalanced Mach-Zehnder interferometer (MZI) (whose arms differ by a time slot period τ). Therefore, the chaos-perturbed data word in N time slots are reconstructed from the decoded MPPM and LDPSK bits. Now, the R-SPU, running a routine for two-dimensional chaotic map precisely matched to that at the transmitter, is solely able to recover the raw data frame initially fed to the transmitter.

C. Non-Synchronized Receiver

One disadvantage of the synchronized receiver is that the decoding of phase information relies mainly on the correct decision of the position information. Therefore, the errors in position information induce corresponding errors in phase information. The main difference proposed in the non-synchronized scheme is that the two decoding processes are made entirely independent, i.e., the decoding of phase information dispenses with the active polarization switching based on MPPM information.

In the non-synchronized receiver, shown in Fig. 2(b), the MPPM decoding is the same as in the synchronized one, and a polarizer added to the LDPSK arm transmits only light polarized at 45° (measured with respect to the x-polarization). Now, both x- and y-polarizations of the received signal contribute equally to the diagonal polarization component. The phase information can be then obtained using a subsequent MZI(s) system as in the synchronized case. While the non-synchronized scheme enables the elimination of MPPM-induced errors in phase information, one notices that only half of the optical signal power delivered to the LDPSK arm is involved in the decision stage. The recovery of original raw data frame is then performed like the case of synchronized receiver.

Here in the transmitter and the receiver implementations (synchronized and non-synchronized variants), the ancillary polarization degree of freedom is employed to dispense with the phase-preserving multi-stage optical delay line used in [9], [10]. While the complexity is obviously reduced via replacing the elements of the k delay stages (required for 2^k time slots per frame) with either a polarization switch or a 45° polarizer, the complexity reduction is also done by avoiding the matching requirements of several optical elements for sake of the phase preservation.

D. Chaotic Perturbations in Position and Phase

To secure the hybrid PA.LDPSK-MPPM signaling, a two-dimensional chaotic map is employed in the transmitter and receiver in order to generate two independent chaotic sequences. One of the two sequences introduces chaotic perturbations in the positions of signal time-slots within the MPPM frame, while the other perturbs the LDPSK phases between consecutive time-slots, with the chaotic attractors P and Φ, receptively. This secret two-dimensional chaotic map along with a common reference clock are shared by T-SPU and R-SPU in order to synchronously iterate and produce identical chaotic outputs. Therefore, the transmitter and receiver systems can precisely encode and decode the chaotic perturbations simultaneously in both position and phase.

Various two-dimensional maps are suited for introducing chaotic perturbations in the proposed systems such as Henon, Lozi, Duffing, and Zaslavsky maps [58]. The values of Lyapunov exponents of the chaotic system quantify the degree of complexity and the dimension of its chaotic attractor [58]. The parameters of chaotic map can be also considered as secret keys for secure communication system. Thus, the chaotic map utilized in proposed system should be a multi-parameter map possessing a large positive Lyapunov exponent to improve the security level of the system. A Zaslavsky map, described by [58], [59]

$$p_i = (p_{i-1} + \kappa\phi_{i-1} + \vartheta) \mod 1, \tag{1}$$

$$\phi_i = \cos(2\pi p_{i-1}) + \exp(-r)\phi_{i-1}, \tag{2}$$

with κ, ϑ and r being positive constants, has a relatively large Lyapunov exponent. It approximately equals 3.5865 compared with less than 0.5 for the other mentioned two-dimensional maps, at $\vartheta = 400$, $\kappa = 12.6695$, and $r = 3$ [59], [60]. Therefore, it exhibits more complex dynamics and excellent statistical properties which lead to the high randomness.

To further increase the output randomness of the chaotic map, both (1) and (2) are seeded by the previous frame information bits. This renders the chaotic output of the system also sensitive to the message information along with the parameters and initial conditions of the chaotic map. The message-seeded Zaslavsky map can then be written as

$$P_i = \rho\left(p_{i-1} + \kappa\phi_{i-1} + \beta_1 d_{1(i-1)} + \vartheta\right) \mod N, \tag{3}$$

$$\Phi_i = \cos(2\pi p_{i-1}) + \exp(-r)\phi_{i-1} + \beta_2 d_{2(i-1)} + \zeta, \tag{4}$$

where ρ, ζ, β_1, and β_2 are positive constants that are kept secret. Here, $d_{1(i-1)}$ and $d_{2(i-1)}$ are predetermined real values corresponding to the specific form of information bits that are encoded and transmitted/received in the previous frame.

While the message-seeded map offers higher security level, mismatches in the discrete chaos may take place due to the information errors induced by the FSO channel noise. Therefore, we propose here that the chaotic parameters are periodically reset every $\mathcal{N}$ frames in order to limit the effect of the chaos mismatch on the bit-error rate of the communication system, with the same initial condition being reused after reset. In this case, the dependence of chaotic perturbations and the frame information helps avoiding the reproduction of similar chaotic perturbations after the reset of the chaotic map system.

The T-SPU runs w iterations of the two-dimensional map per frame and perturbs each phase's bit in a one-by-one fashion by the corresponding value of the chaotic attractors, Φ_i, while the occupied positions of the signal slots are collectively perturbed in a circular displacement by the chaotic value P_i (i.e., circularly shifted within MPPM frame as a group).

Here, the values of secret keys including parameters and initial conditions are kept fixed and known to both sides prior to the encoding process. Moreover, the floating-point precision is set to an identical predetermined accuracy on both sides in

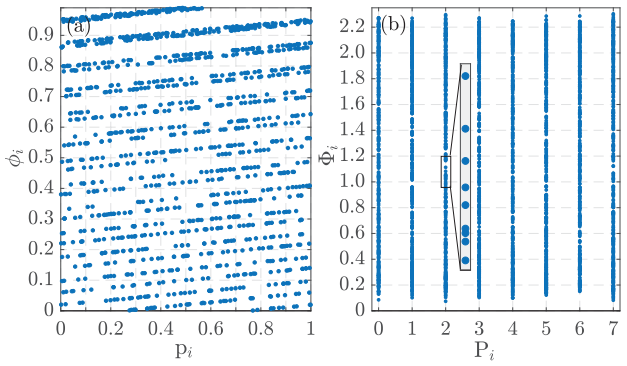

Fig. 3. Numerical results at $\vartheta = 400$, $\kappa = 12.6695$, and $r = 3$ showing (a) distribution of chaotic attractors (p_i, and ϕ_i) of the map (1)–(2), and (b) distribution of modified message-seeded chaotic attractors (P_i, and Φ_i) of the modified map (3)–(4) at $\rho = 1000$, $\beta_1 = 0.0300$, $\beta_2 = 0.0200$, $\zeta = 1.1000$, and $N = 8$.

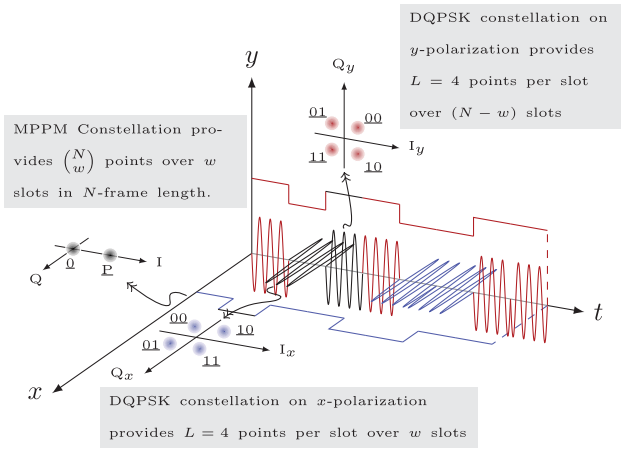

Fig. 4. Constellation diagram of the proposed PA.*L*DPSK-MPPM modulation technique with $N = 8$, $w = 5$, and $L = 4$. I and Q donate the in-phase and quadrature components, respectively.

order to treat the high sensitivity of the chaotic systems to initial conditions. In numerical simulations, the initial conditions used by T-SPU and R-SPU are $(P_0, \Phi_0) = (0.65, 0.79)$.

Figure 3 displays the chaotic attractors of the original Zaslavsky map (p_i and ϕ_i), discrete position perturbing values P_i, and continuous values of phase perturbing values Φ_i for random information data bits. It is obvious that chaotic perturbations are distributed in a unit square in the original map yielding non-reproducible chaotic perturbations for position and phase from the modified map. This also shows the key advantages of the modified chaotic system relative to traditional non-chaotic pseudo random number generators which may generate reproducible random numbers after observation for long periods.

The proposed chaos-based communication system is a peer-to-peer (P2P) transmission method which can be readily extended to multi-user star realizations as follows. In the hub side, there are predetermined different initial conditions utilized in the modified Zaslavsky map such that a specific initial condition is allocated to each user, with the reference clock being shared by all users. The transmitted information bits in the previous frame of a specific user U, along with their associated perturbations in position and phase are saved to be used in the map next time the user U receives data.

Now, let us compare the proposed PA.*L*DPSK-MPPM scheme with one of the recent chaos-based schemes, specifically, the non-coherent PI-DCSK scheme [54]. The PI-DCSK is a secure, energy- and spectrally-efficient modulation technique, in which the data frame is composed of two time slots. First time slot is used to transmit a reference chaotic signal and the second one is used to transmit a permuted replica of the reference signal multiplied by the modulating bit. Compared to this scheme, the chaotic PA.*L*DPSK-MPPM proposed here has the advantage of higher transmission data rate since the reference chaotic signal is produced locally at the two channel terminals with no need for continuous sharing. In addition, sending the reference signal over wireless channel may be a vulnerability degrading the security strength. On the other hand, the chaotic message-seeded reference produced locally in the chaotic PA.*L*DPSK-MPPM leads, as we have discussed, to additional data errors.

IV. Spectral Efficiency Analysis

The utilization of the system bandwidth is measured by the spectral efficiency η, defined as [61]

$$\eta \overset{\text{def}}{=} \frac{\log_2 V}{D/2} \quad \text{bit/sym/pol}, \tag{5}$$

where D is the dimensional of amplitude vector, which is realized by polarization, different time-slots in MPPM scheme, and both components (quadrature and in-phase) of *L*DPSK scheme. PA.*L*DPSK-MPPM scheme has an overall dimension $D = 4N$, which can be factorized into: 2 due to *L*DPSK, 2 given by the state of polarization, and N for the N time slots in MPPM. Furthermore, V is the number of constellation vectors (or symbols). From Fig. 4, V equals $L^N\binom{N}{w}$ for PA.*L*DPSK-MPPM because *L*DPSK provides N transmitted symbols per hybrid frame in addition to $\binom{N}{w}$ symbols from MPPM scheme. However, traditional *L*DPSK-MPPM has $D = 2N$ and $V = L^w\binom{N}{w}$. Therefore, the spectral efficiencies of the PA.*L*DPSK-MPPM and the traditional *L*DPSK-MPPM techniques are given by

$$\begin{aligned} \eta_{\text{PA.}L\text{DPSK-MPPM}} &= \frac{N\log_2 L + \left\lfloor \log_2 \binom{N}{w} \right\rfloor}{2N} \quad \text{bit/sym/pol}, \\ \eta_{L\text{DPSK-MPPM}} &= \frac{w\log_2 L + \left\lfloor \log_2 \binom{N}{w} \right\rfloor}{N} \quad \text{bit/sym/pol}, \end{aligned} \tag{6}$$

respectively.

V. Performance Analysis Under Gamma-Gamma Turbulent FSO Channel

In this section, we obtain expressions for the BERs of proposed systems under gamma-gamma (GG) turbulent channels. In addition, the chaos effect on the BERs is investigated.

A. Gamma-Gamma Turbulent FSO Channel

The performance of FSO communications mainly suffers from atmospheric turbulence which may lead to random fluctuations in both the phase and the amplitude of the received optical signal, which degrades the system performance. Several statistical models have been proposed to investigate the atmospheric effects on FSO transmission [62], [63]. Among them is the gamma-gamma (GG) distribution, which has been shown to be valid in all turbulence regimes for a point receiver [63], [64]. The GG probability density function (pdf) is expressed as [62]

$$f_h(h) = \frac{2(\alpha\beta)^{\frac{\alpha+\beta}{2}}}{\Gamma(\alpha)\Gamma(\beta)} h^{\frac{\alpha+\beta}{2}-1} \mathcal{K}_{\alpha-\beta}\left(2\sqrt{\alpha\beta h}\right), \quad (7)$$

where $\mathcal{K}_s(\cdot)$ is modified Bessel function of second kind of order s. α and β are scintillation parameters, expressed as

$$\alpha = \left(\exp\left(0.49\sigma_R^2/\left(1+1.11\sigma_R^{\frac{12}{5}}\right)^{\frac{7}{6}}\right)-1\right)^{-1}, \quad (8)$$

$$\beta = \left(\exp\left(0.51\sigma_R^2/\left(1+0.69\sigma_R^{\frac{12}{5}}\right)^{\frac{5}{6}}\right)-1\right)^{-1}, \quad (9)$$

respectively, where $\sigma_R^2 = 1.23\ C_n^2(2\pi/\lambda)^{\frac{7}{6}} d^{\frac{11}{6}}$ is unitless Rytov variance, C_n^2 is the refractive-index structure parameter, d is the FSO propagation distance, and λ is the operating wavelength.

B. Net BER of PA.LDPSK-MPPM Systems

1) BER for Synchronized PA.LDPSK-MPPM: An upper bound of average BER for the synchronized (S) PA.LDPSK-MPPM setup is expressed as [9], [10], [13], [14]

$$\begin{aligned}&\mathrm{BER}^{av}_{\text{(S)PA.}L\text{DPSK-MPPM}}\\ &\le \frac{1}{K+N\log_2\ L}\Bigg\{\frac{\mathrm{SER}^{av}_{\text{MPPM}}}{2}\\ &\quad\times\left(\frac{K2^K}{2^K-1}+N\log_2\ L\right)+(1-\mathrm{SER}^{av}_{\text{MPPM}})\log_2\ L\\ &\quad\times\left[\left(\frac{1}{2}-\mathrm{BER}^{av}_{\text{PA.}L\text{DPSK}}\right)\mathrm{SER}^{av}_{\text{MPPM}}+N\,\mathrm{BER}^{av}_{\text{PA.}L\text{DPSK}}\right]\Bigg\},\end{aligned} \quad (10)$$

where $K = \left\lfloor \log_2 \binom{N}{w} \right\rfloor$ is the number of bits/frame encoded using MPPM scheme, $\mathrm{BER}^{av}_{\text{PA.}L\text{DPSK}}$ is the average bit-error rate of PA.LDPSK data bits, and $\mathrm{SER}^{av}_{\text{MPPM}}$ is the average symbol-error rate of MPPM data, which is defined in terms of the $\mathrm{BER}^{av}_{\text{MPPM}}$ as [9], [13]

$$\mathrm{SER}^{av}_{\text{MPPM}} = \frac{2(2^K-1)}{2^K}\,\mathrm{BER}^{av}_{\text{MPPM}}. \quad (11)$$

2) BER of Non-Synchronized PA.LDPSK-MPPM: As mentioned in Subsection III-C for non-synchronized (NS) PA.LDPSK-MPPM, the dependence of PA.LDPSK detection on the MPPM one is removed. Thus, both MPPM and PA.LDPSK detections are completely independent. Therefore, the upper bound of average BER for non-synchronized PA.LDPSK-MPPM techniques can be expressed as

$$\begin{aligned}&\mathrm{BER}^{av}_{\text{(NS)PA.}L\text{DPSK-MPPM}}\\ &\le \frac{K\,\mathrm{BER}^{av}_{\text{MPPM}}+N\log_2\ L\,\mathrm{BER}^{av}_{\text{PA.}L\text{DPSK}}}{K+N\log_2 L},\end{aligned} \quad (12)$$

where the first and second terms of the nominator is related to the probabilities of error of MPPM and PA.LDPSK schemes, respectively, and will be calculated from (21).

3) Average BER Over Gamma-Gamma FSO Channels: The upper-bound BER for both the combined ordinary modulation techniques (PA.LDPSK, and MPPM) are derived based on the maximum-likelihood decoding. Thus the union-bound expression is expressed as [65, CH. 5, PP. 335]

$$\mathrm{BER} \le \frac{\mathcal{C}}{4}\,\mathrm{erfc}\left(\frac{d_{\min}}{2\sqrt{N_0}}\right), \quad (13)$$

where $N_0/2$ is the power spectral density of the noise, and $\mathcal{C}$ is the cardinality of the constellation that are expressed as $\binom{N}{w}$ and L for MPPM and LDPSK modulation, respectively. $d_{\min}$ is the minimum Euclidean distance between two points $[x(t)$ and $z(t)]$ in the constellation space $S(t)$, which is obtained as [65, CH. 5, PP. 335]

$$d^2_{\min} = \min_{\substack{x(t),z(t)\in S\\ x(t)\neq z(t)}}\left\{\int_0^T |x(t)-z(t)|^2\,\mathrm{d}t\right\}. \quad (14)$$

By applying the above expression to the signal constellation set at the photo-detector (PD) output in the receiver port, we take the effects of the PD and the FSO channel gain. Thus, the expression of $d_{\min}$ for different modulation techniques are given as

$$d_{\min}(h) = \sqrt{\frac{\tau}{2}}\mathcal{R}hP\mathcal{Z}_{\text{mod}}, \quad (15)$$

where τ is the slot time duration, $\mathcal{R}$ is the detector responsivity, P is the average transmitted power, with $\mathcal{Z}_{\text{mod}}$ depending on the modulation schemes as

$$\mathcal{Z}_{\text{mod}} = \begin{cases}\frac{1}{2}; & \text{for MPPM in old } L\text{DPSK-MPPM},\\ 1; & \text{for MPPM in PA.}L\text{DPSK-MPPM},\\ \frac{1}{2}\sin(\pi/L); & \text{for } L\text{DPSK},\\ \sin(\pi/L); & \text{for (S)PA.}L\text{DPSK},\\ \frac{1}{2}\sin(\pi/L); & \text{for (NS)PA.}L\text{DPSK}.\end{cases} \quad (16)$$

Thus, by substituting in (13), the upper-bound BER for each modulation scheme can be written as function of channel gain h as

$$\mathrm{BER}_{\text{mod}}(h) \le \frac{\mathcal{C}}{4}\,\mathrm{erfc}\left(\frac{\mathcal{R}}{4}\frac{P}{\sigma}\mathcal{Z}_{\text{mod}}h\right), \quad (17)$$

where $\sigma^2 = N_0/(2\tau)$ is the noise variance, and mod $\in$ { MPPM, LDPSK, (S)PA.LDPSK, (NS)PA.LDPSK}. The average $\mathrm{BER}^{av}_{\text{mod}}$ for every modulation technique can be obtained through

$$\mathrm{BER}^{av}_{\text{mod}} = \int_0^\infty \mathrm{BER}_{\text{mod}}(h) f_h(h)\,\mathrm{d}h. \quad (18)$$

By substituting from (7) and (17) into (20), we get

$$\mathrm{BER}_{\mathrm{mod}}^{av} = \frac{\mathcal{C}}{2}\frac{(\alpha\beta)^{\frac{\alpha+\beta}{2}}}{\Gamma(\alpha)\Gamma(\beta)}\int_0^{\infty} h^{\frac{\alpha+\beta}{2}-1}\,\mathrm{erfc}\left(\frac{\mathcal{R}}{4}\frac{P}{\sigma}\mathcal{Z}_{\mathrm{mod}}h\right) \times\mathcal{K}_{\alpha-\beta}\left(2\sqrt{\alpha\beta h}\right)\mathrm{d}h. \quad (19)$$

Using [66, Eqs. (07.34.03.0619.01) and (03.04.26.0006.01)], through expressing $\mathrm{erfc}(x) = \frac{1}{\sqrt{\pi}}\mathrm{G}_{1,2}^{2,0}\left(x^2|_{0,1/2}^{1}\right)$ and $\mathcal{K}_v(\sqrt{x}) = \frac{1}{2}\mathrm{G}_{0,2}^{2,0}\left(\frac{x}{4}|_{v/2,-v/2}^{-;-}\right)$ in terms of MeijerG function, we get

$$\mathrm{BER}_{\mathrm{mod}}^{av} = \frac{\mathcal{C}}{4\sqrt{\pi}}\frac{(\alpha\beta)^{\frac{\alpha+\beta}{2}}}{\Gamma(\alpha)\Gamma(\beta)}\int_0^{\infty} h^{\frac{\alpha+\beta}{2}-1} \times \mathrm{G}_{1,2}^{2,0}\left(\left(\frac{\mathcal{R}}{4}\frac{P}{\sigma}\mathcal{Z}_{\mathrm{mod}}h\right)^2\Big|_{0,\frac{1}{2}}^{1}\right)\mathrm{G}_{0,2}^{2,0}\left(\alpha\beta h\Big|_{\frac{\alpha-\beta}{2},\frac{\beta-\alpha}{2}}^{-,-}\right)\mathrm{d}h. \quad (20)$$

Then, using [66, Eq. (07.34.21.0013.01)], the $\mathrm{BER}_{\mathrm{mod}}^{av}$ can be written as:

$$\mathrm{BER}_{\mathrm{mod}}^{av} \le \frac{\mathcal{C}}{\pi^{\frac{3}{2}}}\frac{2^{\alpha+\beta-4}}{\Gamma(\alpha)\Gamma(\beta)} \times \mathrm{G}_{5,2}^{2,4}\left(\left(\frac{\mathcal{Z}_{\mathrm{mod}}}{\alpha\beta}\right)^2\bar{\gamma}\Big|_{0,\frac{1}{2}}^{\frac{1-\beta}{2},\frac{2-\beta}{2},\frac{1-\alpha}{2},\frac{2-\alpha}{2},1}\right), \quad (21)$$

where $\bar{\gamma} = \left(\mathcal{R}P/\sigma\right)^2$ is the average signal-to-noise ratio. Finally, by substituting from (16) in (21) and then in (10) and (12), the average BER expressions for the proposed hybrid schemes; synchronized and non-synchronized PA.*L*DPSK-MPPM modulation techniques, can be obtained in (22) and (23), respectively. These mathematical expressions show that the non-synchronized scheme provides better performance compared with the synchronized one. This is due to the independence of the *L*DPSK and MPPM detections in the case of non-synchronized system. Furthermore, as shown in (16) assuming the same transmitted power, the minimum Euclidean-distance for the synchronized PA.*L*DPSK-MPPM is doubled compared with that for *L*DPSK-MPPM technique [9], [10]. This leads to better BERs of the PA setups. It is worth mentioning that the average BER of the more complicated *L*DPSK-MPPM modulation technique can be obtained by substituting form (21) in [10, Eq. (5)].

C. BER From Chaos Mismatch

As mentioned in Subsection III-D, to improve the security the modified chaotic attractors is seeded by the sent information. Accordingly, the received frame errors extend to subsequent frames. To avoid this accumulative feature and to give more reliability to the system performance, the chaotic parameters are reset every $\mathcal{N}$ MPPM frames. Thus, the $\mathrm{BER}^{\mathrm{Chaos}}$ expression that include chaos mismatch effect can be formulated as

$$\mathrm{BER}^{\mathrm{Chaos}} = \frac{\mathrm{BER}^{av}}{\mathcal{N}}\sum_{i=0}^{\mathcal{N}-1}(\mathcal{N}-i)\left(1-\mathrm{BER}^{av}\right)^i, \quad (24)$$

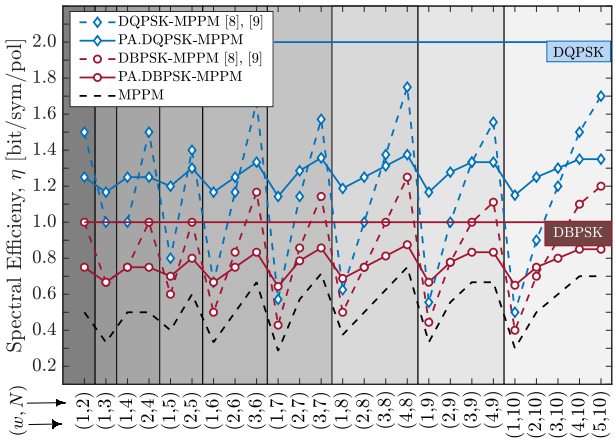

Fig. 5. Comparison between spectral efficiencies of different hybrid *L*DPSK-MPPM schemes over a sequence of frame length N and w active time slots per MPPM frame.

TABLE I
FSO CHANNEL AND SYSTEM PARAMETERS [62], [63]

Parameter	Symbol	Value
Tx/Rx optics efficiency	η	1.0
Photodiode responsivity	$\mathcal{R}$	1.0 A/W
FSO propagation distance	d	5 km
Thermal noise spectral density	$N_{0_{\mathrm{th}}}$	-215 dB/Hz
Time slot duration	τ	2 ns
Operating wavelength	λ	1550 nm

where BER^{av} is net average bit-error rate for synchronized and non-synchronized PA.*L*DPSK-MPPM modulation techniques given in (22) and (23), respectively.

VI. RESULTS AND DISCUSSION

A. Spectral Efficiency Aspects

Figure 5 demonstrates the spectral efficiencies of different hybrid *L*DPSK-based modulation techniques versus the MPPM frame length, N and the number of active time slots per frame, w. It can be noticed that the efficiency of the PA.*L*DPSK-MPPM is always better than the MPPM technique. It can also be more spectrally efficient than the older LDPSK-MPPM implementations, equipped with matched multi-stage delay lines [9], [10], if the set (w, N) is appropriately chosen.

B. BER Performance Aspects

In this subsection, the BER performance of FSO systems adopting hybrid PA.*L*DPSK-MPPM modulation techniques are investigated over GG turbulent FSO channel using the upper-bound BER expressions obtained in (22), (23), [10, Eq. (5)], and (24). Furthermore, the upper bound BERs are verified using Monte Carlo (MC) simulation by directly generating fading states and averaging. The FSO system parameters are listed in Table I [62], [63]. The performance of both proposed synchronized (S), and non-synchronized (NS) setups of PA.*L*DPSK-MPPM techniques are compared to the prior implementations in [9], [10].

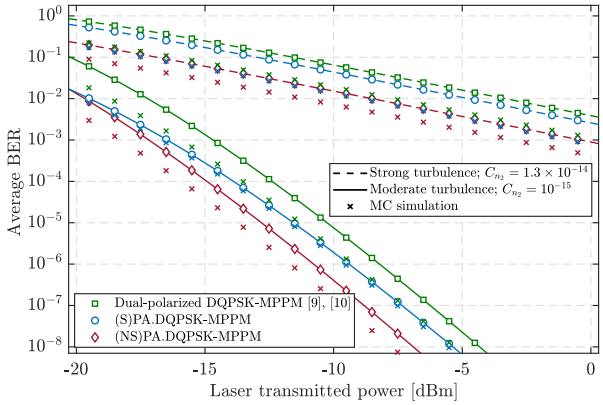

Fig. 6. Average BER versus laser transmitted power [dBm] for different hybrid LDPSK-MPPM schemes at two FSO channel states of $C_{n_2} \in \{1.3 \times 10^{-14}, 10^{-15}\}$. MC simulations are given for each case (denoted by $\times$ in the plot).

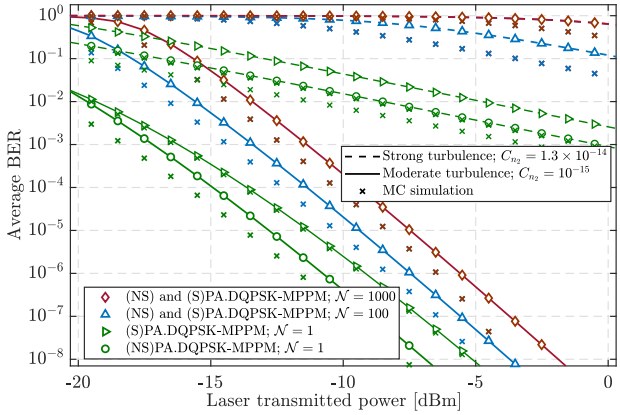

Fig. 7. Average BER due to chaos mismatch versus the laser transmitted power [dBm] for both hybrid PA.LDPSK-MPPM schemes at two FSO channel states of $C_{n_2} \in \{1.3 \times 10^{-14}, 10^{-15}\}$ for different chaos rest duration $\mathcal{N} \in \{1, 10, 100, 1000\}$ MPPM frames. MC simulations are given for each case (denoted by $\times$ in the plot).

For comparison on equal footing, both modulation parameters N and w are chosen from Fig. 5 so as to ensure that all systems have the same transmission data rate and bandwidth, e.g., $(N = 9, w = 3, L = 4)$. In our evaluations, we apply two FSO channel status with different refractive index structure parameters, i.e., $C_{n_2} \in \{1.3 \times 10^{-14}, 10^{-15}\}$ [62], [63].

The comparison of the proposed polarization-assisted techniques with the more complicated LDPSK-MPPM in [10] are illustrated in Fig 6. Using (22), (23), and [10, Eq. (5)], the BERs are depicted versus laser launch optical power for different hybrid LDPSK-MPPM schemes. It is shown that the BERs performance of PA.LDQPSK-MPPM outperform previous LDPSK-MPPM implementations in [9], [10] for different FSO channel status. Specifically, for moderate turbulence FSO status, at a BER of 10^{-3}, the LDPSK-MPPM has a power penalty of $\approx$5 db and 6 db compared with the synchronized and non-synchronized PA.LDPSK-MPPM, respectively. This can be explained as follows: At the same laser transmitted power, the dual-polarized LDPSK-MPPM system has lower optical power per constellation point. This renders the minimum Euclidean distance, $d_{\min}$ as given by (16), and the effective signal-to-noise ratio of the dual-polarized LDPSK-MPPM being reduced (and consequently the BERs performance). Moreover, compared with the other setups, the non-synchronized PA.LDPSK-MPPM system is the most robust against the FSO turbulence. This result can be interpreted by the independence between the MPPM and PA.LDPSK detections in the non-synchronized implementation.

Figure 7 shows the effect of the chaos mismatch on the chaotic PA.LDPSK-MPPM/FSO BER performance. The BERs are plotted for both synchronized and non-synchronized systems for different reset duration of $\mathcal{N} \in \{1, 100, 1000\}$ frames. It is worth mentioning that the case $(\mathcal{N} = 1)$ means that chaos parameters are reset every frame, and this is

$$\begin{aligned}
\mathrm{BER}^{av}_{\text{(S)PA.}L\text{DPSK-MPPM}} \leq\ & \frac{2^{\alpha+\beta-4}}{(K + N\log_2\ L)\pi^{\frac{3}{2}}\Gamma(\alpha)\Gamma(\beta)} \Bigg\{ \binom{N}{w} \mathrm{G}^{2,4}_{5,2}\left(\left(\frac{1}{\alpha\beta}\right)^2 \bar{\gamma}\Big|^{\frac{1-\beta}{2},\frac{2-\beta}{2},\frac{1-\alpha}{2},\frac{2-\alpha}{2},1}_{0,\frac{1}{2}}\right) \\
& \times \left(1 + \frac{N\log_2\ L(2^K-1)}{K2^K}\right) + \log_2 L\left[1 - \frac{2(2^K-1)}{2^K}\binom{N}{w}\mathrm{G}^{2,4}_{5,2}\left(\left(\frac{1}{\alpha\beta}\right)^2 \bar{\gamma}\Big|^{\frac{1-\beta}{2},\frac{2-\beta}{2},\frac{1-\alpha}{2},\frac{2-\alpha}{2},1}_{0,\frac{1}{2}}\right)\right] \\
& \times \Bigg[\mathrm{G}^{2,4}_{5,2}\left(\left(\frac{16}{\alpha\beta}\right)^2 \bar{\gamma}\Big|^{\frac{1-\beta}{2},\frac{2-\beta}{2},\frac{1-\alpha}{2},\frac{2-\alpha}{2},1}_{0,\frac{1}{2}}\right)\left(\frac{1}{2} - L\mathrm{G}^{2,4}_{5,2}\left(\left(\frac{1}{\alpha\beta}\sin\left(\frac{\pi}{L}\right)\right)^2 \bar{\gamma}\Big|^{\frac{1-\beta}{2},\frac{2-\beta}{2},\frac{1-\alpha}{2},\frac{2-\alpha}{2},1}_{0,\frac{1}{2}}\right)\right) \\
& \times \frac{2(2^K-1)}{2^K}\binom{N}{w} + NL\mathrm{G}^{2,4}_{5,2}\left(\left(\frac{1}{\alpha\beta}\sin\left(\frac{\pi}{L}\right)\right)^2 \bar{\gamma}\Big|^{\frac{1-\beta}{2},\frac{2-\beta}{2},\frac{1-\alpha}{2},\frac{2-\alpha}{2},1}_{0,\frac{1}{2}}\right)\Bigg]\Bigg\}, \qquad (22)
\end{aligned}$$

$$\begin{aligned}
\mathrm{BER}^{av}_{\text{(NS)PA.}L\text{DPSK-MPPM}} \leq\ & \frac{2^{\alpha+\beta-4}}{(K + N\log_2 L)\pi^{\frac{3}{2}}\Gamma(\alpha)\Gamma(\beta)} \Bigg[K\binom{N}{w}\mathrm{G}^{2,4}_{5,2}\left(\left(\frac{1}{\alpha\beta}\right)^2 \bar{\gamma}\Big|^{\frac{1-\beta}{2},\frac{2-\beta}{2},\frac{1-\alpha}{2},\frac{2-\alpha}{2},1}_{0,\frac{1}{2}}\right) \\
& + NL\log_2 L\mathrm{G}^{2,4}_{5,2}\left(\left(\frac{1}{2\alpha\beta}\sin\left(\frac{\pi}{L}\right)\right)^2 \bar{\gamma}\Big|^{\frac{1-\beta}{2},\frac{2-\beta}{2},\frac{1-\alpha}{2},\frac{2-\alpha}{2},1}_{0,\frac{1}{2}}\right)\Bigg], \qquad (23)
\end{aligned}$$

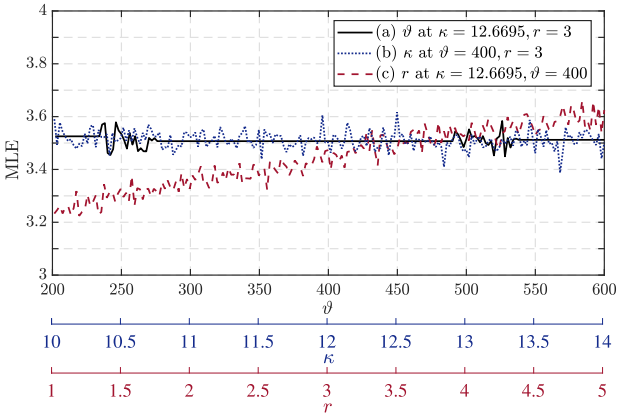

Fig. 8. Maximum Lyapunov Exponent (MLE) plot versus different parameters of Zaslavsky chaotic map for the following cases: (a) $200 \leq \vartheta \leq 600, \kappa = 12.6695, r = 3$, (b) $10 \leq \kappa \leq 14, \vartheta = 400, r = 3$ and (c) $1 \leq r \leq 5, \kappa = 12.6695, \vartheta = 400$.

equivalent to no massage-seeding in the chaotic system operation. It is a theoretical-reference operational-mode with no data-error being generated owing to the chaos mismatch. Thus, this reference case provides the best BER performance compared with the message-seeding cases for $(\mathcal{N} > 1)$. Elongating the reset duration helps improve the security level, however it leads to degradation in system BER performance as shown in Fig. 7. Furthermore, for $(\mathcal{N} > 1)$, the BER performance of the synchronized and non-synchronized PA.LDPSK-MPPM techniques becomes identical. This is interpreted by the dominance of the data errors arising from the chaos mismatch, compared with the ordinary FSO-channel errors. This gives a sort of trade-off behavior between the security due to long-term message-seeding in the chaotic map and the data errors induced by the accumulated chaos mismatch.

C. Security Aspects

The chaos-based image encryption schemes have attracted a great interest during the last two decades (see Refs. [32]–[36] and the references therein). In this subsection, we discuss an example illustrating the advantages of chaotic PA.LDPSK-MPPM. Specifically, we demonstrate the secure transmission of a sample Panda image with dimensions: $X \times Y = 459 \times 459$, fed as information data. The chaotic parameters are $\vartheta = 400$, $\kappa = 12.6695$, $r = 3$, $\rho = 1000$, $\beta_1 = 0.0300$, $\beta_2 = 0.0200$, $\zeta = 1.1000$, and $N = 8$ (the same values set in Fig. 3).

In the security analysis, the numerical values of the parameters are chosen from highly chaotic operational regions in the parameters space. More specifically, the maximum Lyapunov exponent (MLE) is used as an indicator to check for chaos presence and to quantify its strength and complexity. In Fig. 8, the MLE is investigated versus different sections of (ϑ, κ, r) parameters space. It is clear that positive MLEs exist over wide range in parameters space of Zaslavsky map, where appropriate values of secret keys can be selected. The unique secret keys may be initially set for the transmitter and receiver in the manufacturing process. However, in-operation setting of the secret keys can be undertaken using some secured sharing method like quantum key distribution.

The key steps for the secure transfer of the data and the further procedures carried out to confirm its immunity against potential attacks are summarized as follows:

1) The input plain image is used to perturb the values of some secret keys in the secure communication system. The goal of this step is to make the system more immune to different types of differential attacks and confirm that the minute perturbation in the original image will cause a significant difference in the encrypted image.
   Assume that the value of parameter r is chosen from the secret keys of the system to be updated by the input plain image. Then we render it compose from the sum of a secret base value r_0 and a plain image-dependent value $\tilde{r}$ such that:
$$r = r_0 + \tilde{r} = r_0 + c \sum_{i=1}^{X} \sum_{j=1}^{Y} \gamma_{ij}, \tag{25}$$
   where c is a constant, and γ_{ij} is value of the pixel at position (i, j).
2) The plain image is converted to a sequence of data bits. More specifically, for each pixel value there are $8\,\text{bits}$ corresponding to its binary form. The pixels are taken in a row by row order such that they give rise to a stream of $8 \times X \times Y$ bits.

Figure 9 shows the results of numerical simulations when PA.LDPSK-MPPM is applied for secure transmission of Panda image. It can be verified that no critical or meaningful features of the image can be retrieved via conventional statistical attack on the encrypted image. The proposed scheme efficiency against statistical attacks can be studied using histogram analysis. The image histogram is a tool employed to display the distribution of pixels values intensity within a given image. The useful practical encryption scheme must render the transmitted cipher image possess a flat histogram to better immune any statistical attacks.

The resistance against brute force attacks requires that encrypting system has very large number of secret keys that can be utilized in encryption process. The controlled parameters in the modified Zaslavsky map (3)–(4), i.e., ϑ, κ, r, β_1, β_2 and ρ, span continuous ranges of appropriate intervals. Practically, they provide an enormous number of choices that constitute a large key space which is limited only by precision of equipment that controls the parameters values. The sensitivity of secret keys is highlighted in Fig. 9(d) where the value of r is slightly perturbed by adding 10^{-4} to its value while values of other parameters are fixed. It is obvious that the tiny perturbation in secret keys produces significant errors amount in decryption process and yields totally different decrypted image from the original one.

Correlation coefficients between plain and encrypted images can be used to quantify the quality of the encryption process. The efficient secure communications scheme should robustly reduce the correlation between neighboring pixels in all directions. In numerical simulation, we choose a random sample of 10^4 pairs of adjacent pixels in both the original and encrypted images. Then, the correlation coefficients are determined for each color component of the pixels via the

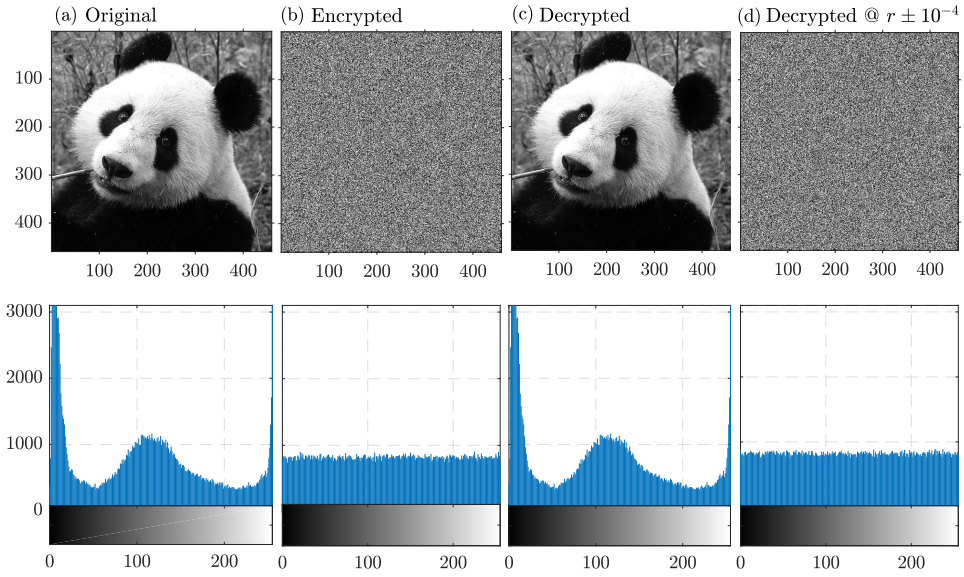

Fig. 9. Sample (panda) image encryption and corresponding histogram for (a) original, (b) encrypted, (c) decrypted, and (d) decrypted image with an error in the value r of $\pm 10^{-4}$, with parameters' values used in Fig. 3.

following relation

$$R_{uv}^{F} = \frac{\sum_{i=1}^{Q}(u_i - \bar{u})(v_i - \bar{v})}{\sqrt{\sum_{i=1}^{Q}(u_i - \bar{u})^2 \sum_{i=1}^{Q}(v_i - \bar{v})^2}}, \tag{26}$$

where u_i and v_i refer to the pixel values of i adjacent pair, F is set as H, V or D for horizontal, vertical or diagonal directions, respectively, and $Q = 10^4$. Also, $\bar{u}$ and $\bar{v}$ refer to the mean intensity of pixels values for the 10^4 selected pairs. Figure 10(a)-(f) shows the correlations in horizontal, vertical, and diagonal directions occur for adjacent pixels in plain images, while the values of correlation coefficients of adjacent pixels (CCAP) are given in Table II.

The resistance of the proposed scheme against differential attacks is examined through applying a slight modification on the particular value of randomly chosen single pixel in original image. A comparison between the resulting encrypted image and the corresponding encrypted image of unperturbed plain image is then carried out. The degree of convergence or divergence between two cipher images can be quantified via the two well-known measurements, namely, the unified average changing intensity (UACI) and the number of pixels change rate (NPCR). The UACI is used measure the mean intensity of differences between two images whereas NPCR evaluates the percentage of different pixel intensities between two images. Both parameters are expressed, respectively, as

$$\text{UACI}\% = \frac{100}{X \times Y} \sum_{i,j} \frac{\gamma_{ij} - \sigma_{ij}}{255}, \tag{27}$$

$$\text{NPCR}\% = \frac{100}{X \times Y} \sum_{i,j} \delta_{ij}, \tag{28}$$

where δ_{ij} is the Kronecker delta, γ_{ij} and σ_{ij} are pixels' values at position (i, j) in first and second encrypted images.

The computed values of UACI and NPCR are shown in Table II. It is clear that CCAP in plain image take large values close to 1, in horizontal, vertical, and diagonal directions. On the other hand, the correlation coefficients between neighboring pixels, in all directions, are obviously reduced in the cipher image. This means that the critical statistical characteristics which depict the original image are diminished in cipher image. Moreover, the large values of UACI and

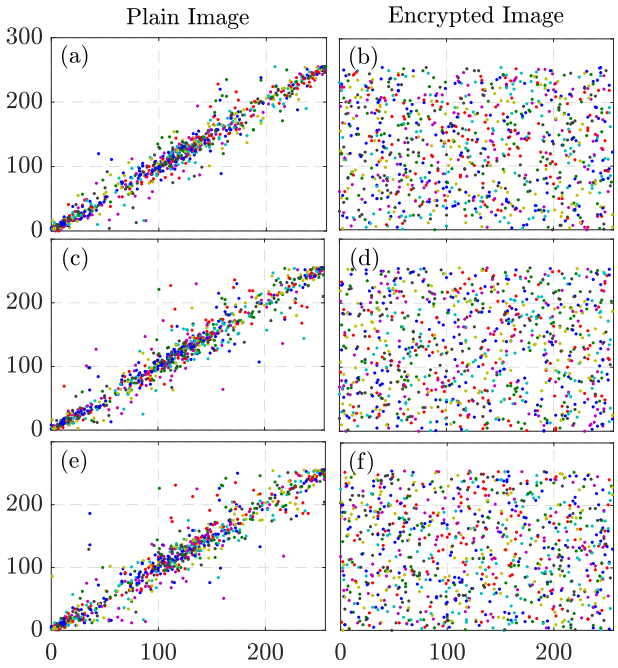

Fig. 10. Correlations between adjacent pixels along: (a) horizontal direction in plain image, (b) horizontal direction in encrypted image, (c) vertical direction in plain image, (d) vertical direction in encrypted image, (e) diagonal direction in plain image, and (f) diagonal direction in encrypted image.

TABLE II

STATISTICAL QUANTITIES WHICH QUANTIFY SECURITY STRENGTH OF THE PROPOSED CHAOS BASED PA.LDPSK-MPPM TECHNIQUE

$R_{uv} = -0.0037$, UACI= 33.476, and NPCR= 99.625			
image	R_{uv}^{H}	R_{uv}^{V}	R_{uv}^{D}
plain	0.9847	0.9773	0.9702
encrypted	−0.0316	0.0325	−0.0239

TABLE III

STATISTICAL QUANTITIES FOR DIFFERENT ZASLAVSKY MAPS THAT ARE USED FOR PROPOSED CHAOTIC PA.*L*DPSK-MPPM TECHNIQUE

Chaotic maps	R_{uv}	UACI	NPCR
(1)–(2)	−0.0037	7.0202	0.0402
(3); position map only	0.1297	18.243	76.512
(4); phase map only	0.1752	12.631	44.780
(3)–(4)	−0.0037	33.4760	99.6250

NPCR highlight the fact that the proposed technique is high sensitive to minute perturbations in input data [36]. Table III shows a comparison of the statistical quantities that justify the security strength of the chaotic maps. We explore the results obtained for different maps; where original Zaslavsky map with ($\beta_1 = \beta_2 = 0$) is utilized along with unperturbed parameter r. The lower the values of NPCR and UACI, the more vulnerable the system to differential attacks. Furthermore, the degradation in the security level is also observed when chaotic perturbations are applied only on the positions of information bits as illustrated.

VII. CONCLUSION

We have presented all-optical setups for hybrid chaos-secured PA.*L*DPSK-MPPM where the optical-signal polarization is employed as an additional degree of freedom to dispense with the matched multi-stage optical-delay lines necessary for the prior systems. The security of the new hybrid modulation scheme is guaranteed by incorporating message-seeded two-dimensional discrete-chaos perturbations in the physical layer. Spectral efficiencies analysis shows competitive data rates of the proposed PA.*L*DPSK-MPPM techniques compared with that of the more complicated prior implementations of *L*DPSK-MPPM. The BER expressions have been determined for the proposed scheme considering fading gamma-gamma FSO channels. Based on these expressions, the system performance has been investigated and compared with that of the prior *L*DPSK-MPPM scheme. The numerical results reveal that the PA.*L*DPSK-MPPM modulation outperforms its prior counterpart implementations of *L*DPSK-MPPM, specifically, with a power saving of at least 5 db at a BER of 10^{-4}. A trade-off has been verified between the chaos-mismatch BER performance and the security level due to the message-seeded two-dimensional chaotic map. The immunity of the chaotic PA.*L*DPSK-MPPM scheme has been checked via numerical analysis by transmitting a sample image. The large key space of the proposed secure communication scheme abolishes the effectiveness of brute-force attacks. The invulnerability of the encrypting system against various statistical attacks is verified through teeny values of correlation coefficients and image histograms. Moreover, the measurements of NPCR and UACI prove the impregnability of the proposed technique versus differential attacks.

REFERENCES

[1] M. A. Khalighi and M. Uysal, "Survey on free space optical communication: A communication theory perspective," *IEEE Commun. Surveys Tuts.*, vol. 16, no. 4, pp. 2231–2258,4th Quart., 2014.

[2] H. Kaushal and G. Kaddoum, "Optical communication in space: Challenges and mitigation techniques," *IEEE Commun. Surveys Tuts.*, vol. 19, no. 1, pp. 57–96, 1st Quart., 2017.

[3] E. Agrell and M. Karlsson, "Power-efficient modulation formats in coherent transmission systems," *J. Lightw. Technol.*, vol. 27, no. 22, pp. 5115–5126, Nov. 15, 2009.

[4] X. Liu *et al.*, "M-ary pulse-position modulation and frequency-shift keying with additional polarization/phase modulation for high-sensitivity optical transmission," *Opt. Express*, vol. 19, no. 26, pp. B868–B881, Dec. 2011.

[5] M. Karlsson and E. Agrell, "Generalized pulse-position modulation for optical power-efficient communication," in *Proc. 37th Eur. Conf. Exhib. Opt. Commun. (ECOC)*, Geneva, Switzerland, Sep. 2011, pp. 1–3.

[6] X. Liu, T. H. Wood, R. W. Tkach, and S. Chandrasekhar, "Demonstration of record sensitivities in optically preamplified receivers by combining PDM-QPSK and M-Ary pulse-position modulation," *J. Lightw. Technol.*, vol. 30, no. 4, pp. 406–413, Feb. 15, 2012.

[7] H. Selmy, H. M. H. Shalaby, and Z.-I. Kawasaki, "Proposal and performance evaluation of a hybrid BPSK-modified MPPM technique for optical fiber communications systems," *J. Lightw. Technol.*, vol. 31, no. 22, pp. 3535–3545, Nov. 2013.

[8] H. S. Khallaf, H. M. H. Shalaby, and Z. Kawasaki, "Proposal of a hybrid OFDM-PPM technique for free space optical communications systems," in *Proc. IEEE Photon. Conf. (IPC)*, Bellevue, WA, USA, Sep. 2013, pp. 287–288.

[9] A. E. Morra, H. M. H. Shalaby, S. F. Hegazy, and S. S. A. Obayya, "Hybrid direct-detection differential phase shift keying-multipulse pulse position modulation techniques for optical communication systems," *Opt. Commun.*, vol. 357, no. 5, pp. 86–94, Dec. 2015.

[10] A. E. El-Fiqi, A. E. Morra, S. F. Hegazy, H. M. H. Shalaby, K. Kato, and S. S. A. Obayya, "Performance evaluation of hybrid DPSK-MPPM techniques in long-haul optical transmission," *Appl. Opt.*, vol. 55, no. 21, pp. 5614–5622, Jul. 2016.

[11] H. M. H. Shalaby, "Maximum achievable constrained power efficiencies of MPPM–*L*QAM techniques," *IEEE Photon. Technol. Lett.*, vol. 27, no. 12, pp. 1265–1268, Jun. 15, 2015.

[12] A. E. Morra, M. Rihan, A. E. El-Fiqi, H. M. H. Shalaby, and S. S. A. Obayya, "Evaluation of power efficiency of hybrid modulation techniques," in *Proc. IEEE Photon. Conf. (IPC)*, Waikoloa, HI, USA, Oct. 2016, pp. 33–34.

[13] H. S. Khallaf, H. M. H. Shalaby, J. M. Garrido-Balsells, and S. Sampei, "Performance analysis of a hybrid QAM-MPPM technique over turbulence-free and gamma-gamma free-space optical channels," *IEEE/OSA J. Opt. Commun. Netw.*, vol. 9, no. 2, pp. 161–171, Feb. 2017.

[14] H. S. Khallaf, A. E. Elfiqi, H. M. H. Shalaby, S. Sampei, and S. S. A. Obayya, "On the performance evaluation of *L*QAM-MPPM techniques over exponentiated Weibull fading free-space optical channels," *Opt. Commun.*, vol. 416, pp. 41–49, Jun. 2018.

[15] R. Essiambre and R. W. Tkach, "Capacity trends and limits of optical communication networks," *Proc. IEEE*, vol. 100, no. 5, pp. 1035–1055, May 2012.

[16] H. V. Poor and R. F. Schaefer, "Wireless physical layer security," *Proc. Nat. Acad. Sci.*, vol. 114, no. 1, pp. 19–26, Jan. 2017.

[17] R. L. Rivest, A. Shamir, and L. Adleman, "A method for obtaining digital signatures and public-key cryptosystems," *Commun. ACM*, vol. 21, no. 2, pp. 120–126, Feb. 1978.

[18] N. Gisin, G. Ribordy, W. Tittel, and H. Zbinden, "Quantum cryptography," *Rev. Mod. Phys.*, vol. 74, p. 145, Mar. 2002.

[19] S. J. Devitt, "Performing quantum computing experiments in the cloud," *Phys. Rev. A, Gen. Phys.*, vol. 94, no. 3, Sep. 2016, Art. no. 032329.

[20] L. Keuninckx, M. C. Soriano, I. Fischer, C. R. Mirasso, R. M. Nguimdo, and G. Van der Sande, "Encryption key distribution via chaos synchronization," *Sci. Rep.*, vol. 7, Feb. 2017, Art. no. 43428.

[21] A. Argyris *et al.*, "Chaos-based communications at high bit rates using commercial fibre-optic links," *Nature*, vol. 438, no. 7066, p. 343, Nov. 2005.

[22] N. F. Rulkov, M. M. Sushchik, L. S. Tsimring, and A. R. Volkovskii, "Digital communication using chaotic-pulse-position modulation," *IEEE Trans. Circuits Syst. I, Fundam. Theory Appl.*, vol. 48, no. 12, pp. 1436–1444, Dec. 2001.

[23] A. E. Morra, S. F. Hegazy, A. Elsonbaty, and S. S. Obayya, "Chaotic DPSK-MPPM modulation technique for a physically secure and highly robust optical communication system," in *Proc. IEEE/ACES Int. Conf. Wireless Inf. Technol. Syst. (ICWITS), Appl. Comput. Electromagn. (ACES)*, Honolulu, HI, USA, Mar. 2016, pp. 1–2.

[24] M. Z. Chowdhury, M. T. Hossan, A. Islam, and Y. M. Jang, "A comparative survey of optical wireless technologies: Architectures and applications," *IEEE Access*, vol. 6, pp. 9819–9840, 2018.
[25] (2014). *International Atomic Energy Agency (IAEA)*. [Online]. Available: https://www.iaea.org/projects/crp/i31028
[26] M. L. Sichitiu and M. Kihl, "Inter-vehicle communication systems: A survey," *IEEE Commun. Surveys Tuts.*, vol. 10, no. 2, pp. 88–105, Jul. 2008.
[27] H. S. Khallaf and H. M. H. Shalaby, "Proposal of a hybrid QAM-MPPM technique for optical communications systems," in *Proc. 16th Int. Conf. Transparent Opt. Netw. (ICTON)*, Graz, Austria, Jul. 2014, pp. 1–4.
[28] G. Kaddoum, "Wireless chaos-based communication systems: A comprehensive survey," *IEEE Access*, vol. 4, pp. 2621–2648, May 2016.
[29] A. Argyris, E. Grivas, A. Bogris, and D. Syvridis, "Transmission effects in wavelength division multiplexed chaotic optical communication systems," *J. Lightw. Technol.*, vol. 28, no. 21, pp. 3107–3114, Nov. 1, 2010.
[30] Y. Hong, M. W. Lee, J. Paul, P. S. Spencer, and K. A. Shore, "GHz bandwidth message transmission using chaotic vertical-cavity surface-emitting lasers," *J. Lightw. Technol.*, vol. 27, no. 22, pp. 5099–5105, Nov. 15, 2009.
[31] S. Y. Xiang *et al.*, "Message encoding/decoding using unpredictability-enhanced chaotic VCSELs," *IEEE Photon. Technol. Lett.*, vol. 24, no. 15, pp. 1267–1269, Aug. 1, 2012.
[32] C. Li, G. Luo, K. Qin, and C. Li, "An image encryption scheme based on chaotic tent map," *Nonlinear Dyn.*, vol. 87, no. 1, pp. 127–133, 2017.
[33] W. Wen, Y. Zhang, M. Su, R. Zhang, J.-X. Chen, and M. Li, "Differential attack on a hyper-chaos-based image cryptosystem with a classic bi-modular architecture," *Nonlinear Dyn*, vol. 87, no. 1, pp. 383–390, Jan. 2017.
[34] L. Chen, B. Ma, X. Zhao, and S. Wang, "Differential cryptanalysis of a novel image encryption algorithm based on chaos and Line map," *Nonlinear Dyn.*, vol. 87, no. 3, pp. 1797–1807, Feb. 2017.
[35] Y. Li, C. Wang, and H. Chen, "A hyper-chaos-based image encryption algorithm using pixel-level permutation and bit-level permutation," *Opt. Lasers Eng.*, vol. 90, pp. 238–246, Mar. 2017.
[36] Y. Xie, J. Li, Z. Kong, Y. Zhang, X. Liao, and Y. Liu, "Exploiting optics chaos for image encryption-then-transmission," *J. Lightw. Technol.*, vol. 34, no. 22, pp. 5101–5109, Nov. 15, 2016.
[37] A. Uchida *et al.*, "Fast physical random bit generation with chaotic semiconductor lasers," *Nature Photon.*, vol. 2, no. 12, pp. 728–732, 2008.
[38] R. Sakuraba, K. Iwakawa, K. Kanno, and A. Uchida, "Tb/s physical random bit generation with bandwidth-enhanced chaos in three-cascaded semiconductor lasers," *Opt. Express*, vol. 23, no. 2, pp. 1470–1490, 2015.
[39] A. Elsonbaty, S. F. Hegazy, and S. S. A. Obayya, "A new technique for ultrafast physical random number generation using optical chaos," *Proc. SPIE*, vol. 9892, Apr. 2016, Art. no. 98921P.
[40] A. Elsonbaty, S. F. Hegazy, and S. S. A. Obayya, "Numerical analysis of ultrafast physical random number generator using dual-channel optical chaos," *Opt. Eng.*, vol. 55, no. 9, Sep. 2016, Art. no. 094105. doi: 10.1117/1.OE.55.9.094105.
[41] F.-Y. Lin and J.-M. Liu, "Chaotic lidar," *IEEE J. Sel. Topics Quantum Electron.*, vol. 10, no. 5, pp. 991–997, Sep./Oct. 2004.
[42] Y. SenLin, "Chaotic synchronization of two mutually coupled semiconductor lasers for optoelectronic logic gates," *Commun. Nonlinear Sci. Numer. Simul.*, vol. 17, no. 7, pp. 2896–2904, Jul. 2012.
[43] A. Elsonbaty, S. F. Hegazy, and S. S. A. Obayya, "Simultaneous suppression of time-delay signature in intensity and phase of dual-channel chaos communication," *IEEE J. Quantum Electron.*, vol. 51, no. 9, Sep. 2015, Art. no. 2400309.
[44] A. Elsonbaty, S. F. Hegazy, and S. S. A. Obayya, "Simultaneous concealment of time delay signature in chaotic nanolaser with hybrid feedback," *Opt. Lasers Eng.*, vol. 107, pp. 342–351, Aug. 2018.
[45] A. Elsonbaty, S. F. Hegazy, and S. S. A. Obayya, "Suppressed time delay signature in chaotic nanolasers with hybrid feedback," *Proc. SPIE*, vol. 10682, May 2018, Art. no. 106821Q.
[46] A. Elsonbaty, S. F. Hegazy, and S. S. A. Obayya, "Time delay signature of chaotic nanolasers and its concealment," in *Proc. Int. Appl. Comput. Electromagn. Soc. Symp.-Italy (ACES)*, Mar. 2017, pp. 1–2.
[47] G. Kolumbán, M. Kennedy, and G. Kis, "Performance improvement of chaotic communications systems," in *Proc. Eur. Conf. Circuit Theory Design (ECCTD)*, Budapest, Hungary, Aug./Sep. 1997, pp. 284–289.
[48] H. Dedieu, M. P. Kennedy, and M. Hasler, "Chaos shift keying: Modulation and demodulation of a chaotic carrier using self-synchronizing Chua's circuits," *IEEE Trans. Circuits Syst. II, Analog Digit. Signal Process.*, vol. 40, no. 10, pp. 634–642, Oct. 1993.
[49] Z. Galias and G. M. Maggio, "Quadrature chaos-shift keying: Theory and performance analysis," *IEEE Trans. Circuits Syst. I, Fundam. Theory Appl.*, vol. 48, no. 12, pp. 1510–1519, Dec. 2001.
[50] G. Kolumbán, B. Vizvári, W. Schwarz, and A. Abel, "Differential chaos shift keying: A robust coding for chaos communication," in *Proc. 4th Int. Workshop Nonlinear Dyn. Electron. Syst. (NDES)*, Seville, Spain, Jun. 1996, pp. 87–92.
[51] G. Cai, Y. Fang, G. Han, L. Wang, and G. Chen, "A new hierarchical M-ary DCSK communication system: Design and Analysis," *IEEE Access*, vol. 5, pp. 17414–17424, 2017.
[52] G. Kaddoum, E. Soujeri, C. Arcila, and K. Eshteiwi, "I-DCSK: An improved noncoherent communication system architecture," *IEEE Trans. Circuits Syst. II, Exp. Briefs*, vol. 62, no. 9, pp. 901–905, Sep. 2015.
[53] G. Kaddoum, E. Soujeri, and Y. Nijsure, "Design of a short reference noncoherent chaos-based communication systems," *IEEE Trans. Commun.*, vol. 64, no. 2, pp. 680–689, Jan. 2016.
[54] M. Herceg, G. Kaddoum, D. Vranješ, and E. Soujeri, "Permutation index DCSK modulation technique for secure multiuser high-data-rate communication systems," *IEEE Trans. Veh. Technol.*, vol. 67, no. 4, pp. 2997–3011, Apr. 2018.
[55] S. F. Hegazy, S. S. A. Obayya, and B. E. A. Saleh, "Orthogonal quasi-phase-matched superlattice for generation of hyperentangled photons," *Sci. Rep.*, vol. 7, 2017, Art. no. 4169.
[56] S. F. Hegazy, Y. A. Badr, and S. S. A. Obayya, "Relative-phase and time-delay maps all over the emission cone of hyperentangled photon source," *Opt. Eng.*, vol. 56, no. 2, 2017, Art. no. 026114. doi: 10.1117/1.OE.56.2.026114
[57] *Versawave Technologies, Polarization Modulators*. (2018). [Online]. Available: http://www.versawave.com/products/polariza tion-modulators
[58] C. Robinson, *Dynamical Systems: Stability, Symbolic Dynamics, and Chaos*, 2nd ed. Boca Raton, FL, USA: CRC Press, 1998.
[59] G. M. Zaslavsky, "The simplest case of a strange attractor," *Phys. Lett. A*, vol. 69, no. 3, pp. 145–147, Dec. 1978.
[60] J. Bovy, "Lyapunov exponents and strange attractors in discrete and continuous dynamical systems," Theoretica Phys. Project, Catholic Univ. Leuven, Flanders, Belgium, Tech. Rep. 9, 2004, pp. 1–19.
[61] S. Benedetto and E. Biglieri, *Principles of Digital Transmission: With Wireless Applications*. New York, NY, USA: Kluwer, 1999.
[62] M. A. Al-Habash, L. C. Andrews, and R. L. Phillips, "Mathematical model for the irradiance probability density function of a laser beam propagating through turbulent media," *Opt. Eng.*, vol. 40, pp. 1554–1562, Aug. 2001.
[63] A. E. Morra, H. S. Khallaf, H. M. H. Shalaby, and Z. Kawasaki, "Performance analysis of both shot- and thermal-noise limited multipulse PPM receivers in gamma–gamma atmospheric channels," *J. Lightw. Technol.*, vol. 31, no. 19, pp. 3142–3150, Oct. 1, 2013.
[64] F. S. Vetelino, C. Young, and L. Andrews, "Fade statistics and aperture averaging for Gaussian beam waves in moderate-to-strong turbulence," *Appl. Opt.*, vol. 46, no. 18, pp. 3780–3789, Jun. 2007.
[65] S. Haykin, *Communication System*, 4th ed. New York, NY, USA: Wiley, 2001.
[66] (Sep. 2017). *Wolfram Function Site*. [Online]. Available: http://functions.wolfram.com/

Abdulaziz E. Elfiqi (S'16–M'17) received the B.Sc. (Hons.) and M.Sc. degrees from the Faculty of Electronic Engineering, Menoufia University, Menouf, Egypt, in 2006 and 2011, respectively, and the Ph.D. degree from the Egypt-Japan University of Science and Technology, Alexandria, Egypt, in 2016, all in electronic and communication engineering. In 2016, he joined the Electronics and Electrical Communications Engineering Department, Faculty of Electronic Engineering, Menoufia University, as an Assistant Professor. From 2015 to 2016, he was with the Graduate School of Information Science and Electrical Engineering, Kyushu University, Japan, as a Visiting Researcher. From 2016 to 2017, he was with the Center of Photonics and Smart Materials, Zewail City of Science and Technology, Egypt, as a Post-Doctoral Fellow. His research interests include optical communications and integrated photonics.

Haitham S. Khallaf received the B.Sc. degree (Hons.) from the Faculty of Electronic Engineering, Menoufia University, Menouf, Egypt, in 2005, and the M.Sc. (Hons.) and Ph.D. degrees from the Egypt-Japan University of Science and Technology (E-JUST), Alexandria, Egypt, in 2013 and 2016, respectively. He is currently a Post-Doctoral Researcher with the Department of Electrical and Electronics Engineering, Ozyegin University, Istanbul, Turkey, on leave from his position as an Assistant Professor at the Nuclear Research Center (NRC), Egyptian Atomic Energy Authority (EAEA), Egypt. From 2016 to 2017, he was a Post-Doctoral Researcher with the Center for Photonics and Smart Materials, Zewail City of Science and Technology. His research interests include channel modeling for free space optical communication systems, unmanned aerial vehicle network backhauling, integration between VLC system and B5G mobile network, and application of wireless communication systems in nuclear facilities.

Salem F. Hegazy was born in Hulwan, Egypt, in 1980. He received the B.Sc. degree (Hons.) in electronics and communications engineering, the Diploma degree in optical systems, and the M.Sc. degree in free-space communications using entangled photons from Cairo University, Egypt, in 2002, 2006, and 2011, respectively, and the Ph.D. degree in quantum optics and nonlinear optics under joint-supervision between CREOL: The College of Optics and Photonics, University of Central Florida, Orlando, FL, USA, and the National Institute of Laser Enhanced Sciences (NILES), Cairo University, in 2017. He is currently an Assistant Professor with the National Institute of Laser Enhanced Sciences, Cairo University, and also a Post-Doctoral Researcher with the Center for Photonics and Smart Materials, Zewail City of Science and Technology. His research interests include integrated quantum information and quantum computation systems, optical communications, and chaos-based systems.

Amr Elsonbaty was born in Egypt in 1984. He received the B.Sc. degree in electronics and communications engineering and the M.Sc. degree in engineering mathematics from Mansoura University, Egypt, in 2006 and 2011, respectively, and the Ph.D. degree in engineering mathematics from Mansoura University, in 2015. Since then, he has been an Assistant Professor with the Mathematics Department, College of Science and Humanities Studies, Prince Sattam Bin Abdulaziz University, Al-Kharj, Saudi Arabia, and also with the Faculty of Engineering, Mansoura University. He was formerly a Post-Doctoral Researcher with the Center for Photonics and Smart Materials, Zewail City of Science and Technology. His current research interests include nonlinear dynamics of electronic circuits, bifurcation theory, chaos control and synchronization, chaos generation utilizing lasers, and chaotic optical communication systems.

Hossam M. H. Shalaby (S'83–M'91–SM'99) was born in Giza, Egypt, in 1961. He received the B.S. and M.S. degrees from Alexandria University, Alexandria, Egypt, in 1983 and 1986, respectively, and the Ph.D. degree from the University of Maryland at College Park, in 1991, all in electrical engineering. In 1991, he joined the Electrical Engineering Department, Alexandria University, and was promoted to Professor in 2001. From 2010 to 2016, he was the Chair of the Department of Electronics and Communications Engineering, Egypt-Japan University of Science and Technology (E-JUST), Alexandria, Egypt. From 1996 to 1998, he was with the Electrical and Computer Engineering Department, International Islamic University Malaysia. He was with the School of Electrical and Electronic Engineering, Nanyang Technological University, Singapore, from 1998 to 2001. His research interests include optical communications, silicon photonics, optical CDMA, and quantum information theory. He is a Senior Member of the IEEE Photonics Society and The Optical Society (OSA).

Salah S. A. Obayya (SM'05) received the B.Sc. (Hons.) and M.Sc. degrees in electronics and communications engineering from Mansoura University, Egypt, in 1991 and 1994, respectively, and the Ph.D. degree from Mansoura University, in 1999. From 1997 to 1999, he was with the Department of Electrical, Electronic, and Information Engineering, City University London, London, U.K., to carry out the research part of his Ph.D. under the joint supervision scheme between the City University London and Mansoura University. From 2000 to 2003, he was a Senior Research Fellow with the School of Engineering, City University London. From 2003 to 2006, he was with the School of Engineering and Design, Brunel University, London, as a Senior Lecturer, and a Reader with the School of Electronic and Electrical Engineering, University of Leeds. Since 2008, he has been a Full Professorial Chair of photonics and led the establishment of the Nano-Photonics Research Centre, The University of Glamorgan, U.K., while he was currently the Vice Chair for Academic Affairs, Zewail City of Science and Technology, Egypt. He has built an outstanding international reputation in the area of green nanophotonics with a focus on the intelligent computational modeling of modern nanophotonic devices enabling technologies for efficient generation, distribution, and utilization of sustainable energy toward low-carbon green society. He has a track record of 232 journal publications mostly in the IEEE, IET/IEE, and OSA; has authored three books, namely *Computational Photonics* (Wiley, 2010), *Computational Liquid Crystal Photonics* (Wiley, 2016), and *Computational of Photonic Sensors* (2018), which are adopted references for Graduate Programs in Photonics at international Universities; and 252 conference papers in international conference in photonics, many of these are invited talks, and keynote lectures, attracted external funding, from both industry and Research Councils, in the region of $4M, and supervised to successful completion 35 Ph.D. students, over 70 M.Sc./M.Res./M.Phil. students, and 15 postdoctoral research fellows.